AIP2020_2

by Leny Yuliati

Submission date: 27-Jul-2022 01:53PM (UTC+0800)
Submission ID: 1875728730
File name: phenol_degradation_Effect_of_precursor_and_salt_melt_amounts.pdf (1.87M)
Word count: 5590
Character count: 26814

Crystalline carbon nitride for photocatalytic phenol degradation: Effect of precursor and salt melt amounts

Cite as: AIP Conference Proceedings **2237**, 020049 (2020); https://doi.org/10.1063/5.0005795
Published Online: 02 June 2020

Leny Yuliati, Mohd Hayrie Mohd Hatta, Siew Ling Lee, and Hendrik O. Lintang

Crystalline Carbon Nitride for Photocatalytic Phenol Degradation: Effect of Precursor and Salt Melt Amounts

Leny Yuliati[1, 2, 3, a)], Mohd Hayrie Mohd Hatta[4, b)], Siew Ling Lee[3, 4, c)] and Hendrik O. Lintang[1, 2, 3, d)]

[1]*Ma Chung Research Center for Photosynthetic Pigments, Universitas Ma Chung, Villa Puncak Tidar N-01, Malang 65151, East Java, Indonesia*
[2]*Department of Chemistry, Faculty of Science and Technology, Universitas Ma Chung, Villa Puncak Tidar N-01, Malang 65151, East Java, Indonesia*
[3]*Centre for Sustainable Nanomaterials, Ibnu Sina Institute for Scientific and Industrial Research, Universiti Teknologi Malaysia, 81310 Johor Bahru, Johor, Malaysia*
[4]*Department of Chemistry, Faculty of Science, Universiti Teknologi Malaysia, 81310 Johor Bahru, Johor, Malaysia*

[a)]Corresponding author: leny.yuliati@machung.ac.id
[b)]mhayrie2@gmail.com
[c)]sllee@ibnusina.utm.my
[d)] hendrik.lintang@machung.ac.id

Abstract. Development of visible-light-active photocatalyst is an important approach to utilize solar energy in the future. The attempts to improve the crystallinity of photocatalyst have been the focus of the research. Recently, the use of potassium chloride-lithium chloride (KCl-LiCl) salt melt has been reported to increase the crystallinity of carbon nitride. In this work, precursor and salt melt amounts were varied to study the properties and the photocatalytic activity of the crystalline carbon nitride for phenol degradation. When the precursor amount was too low (1 g), no product was obtained due to the decomposition of precursor. When it was too high (4 g), the product showed the characters of amorphous CN. Optical properties also showed that when the precursor amount was 3–4 g, the incomplete condensation process occurred and defects were formed due to the excessive washing. The specific surface area also decreased with the increase of the precursor amount from 2 to 4. When the amount of salt melt was too low (2.5 g), the crystalline CN could not be obtained. However, when the amount of salt melt was increased to 7.5 g, impurities could not be avoided. Longer time and multiple washing processes were required in order to remove the impurities, which certainly affected the crystallinity. Photocatalytic activity test showed that the high activity was obtained on the sample prepared using the optimum amount of precursor (2 g) and salt melt (5 g), which would be due to the high crystallinity and large specific surface area.

INTRODUCTION

Phenol is known to be a toxic molecule and the permission exposure level in bottle water has been set to 0.001 mg/L by the Food and Drug Administration (FDA), while the Occupational Safety and Health Administration (OSHA) has set the legal limit of phenol in air to 5 ppm over an 8-hour work day [1]. While various methods have been reported to treat phenol, one promising approach that is worth to be explored is by photocatalytic reaction. The photocatalytic degradation of phenol has been shown to provide the environmentally safe pathway and the process in principle only needs the light energy and suitable semiconductor photocatalyst [2-4].

In order to fully utilize the abundant solar light, the photocatalyst shall be able to absorb the visible light which is larger part than the ultra violet (UV) region in the solar spectrum. Carbon nitride has been recognized as an organic semiconductor that could work as a potential heterogeneous photocatalyst under visible light irradiation [5-7]. While many methods have been developed to synthesize carbon nitride, most of them are in amorphous form. However,

The 14th Joint Conference on Chemistry 2019
AIP Conf. Proc. 2237, 020049-1–020049-10; https://doi.org/10.1063/5.0005795
Published by AIP Publishing. 978-0-7354-1996-4/$30.00

amorphous carbon nitride usually shows less photocatalytic activity than the crystalline carbon nitride, either for photocatalytic hydrogen production [8] or photocatalytic degradation of organic pollutant such as phenol [9]. Therefore, the development of methods to synthesize crystalline carbon nitride is still an emerging research in this photocatalytic field. Recently, our group reported the use of potassium chloride-lithium chloride (KCl-LiCl) salt melt to synthesize crystalline carbon nitride [9]. In this study, we further investigated the effects of precursor amount and salt melt amount on the properties and photocatalytic activity of the obtained carbon nitride.

EXPERIMENTAL

The crystalline carbon nitride samples were prepared in the similar way to the previous report [9]. The precursor of carbon nitride was prepared by calcining a certain amount of urea (CH_4N_2O, QRëC, 99%, 30 g) at 350 °C for 6 hours. In order to investigate the effect of the precursor amount, 2–4 g of precursor was added to 30 mL of ethanol solvent, followed by continuous stirring at 100 °C until all ethanol solvent was successfully evaporated. The obtained solid precursor was transferred to a porcelain mortar. A certain amount of salt melt (5 g), which was potassium chloride (KCl, Fisher Chemicals, 99.5%, 2.74 g) and lithium chloride (LiCl, Sigma-Aldrich, 99%, 2.26 g), was added into the mortar and the mixture was then ground together. The mixture was then heated at a ramp of 2.2 °C/min to reach 550 °C in a muffle furnace. The heating at 550 °C was held for 4 hours before cooling it to room temperature. The final product was ground to powder and the washing process was performed to remove residual salts with boiling water. The final products were labeled as x–CN, which x refers to 2, 3, and 4 g. To study the effect of the salt melt amount, a similar synthesis method was performed. The amounts of precursor (2 g), reaction temperature (550 °C), and reaction time (4 hours) were fixed, while the amount of salt melt was varied to 2.5 g (1.37 g KCl, 1.13 g LiCl), 5 g (2.74 g KCl, 2.26 g LiCl), and 7.5 g (4.11 g KCl, 3.39 LiCl). The final products were labeled as CN–x, which x refers to 2.5, 5, and 7.5 g of salt melt.

All the samples were further characterized by X-ray diffractometer (XRD, Bruker D8 Advance), diffuse reflectance ultraviolet-visible (DR UV-vis, Shimadzu UV-2600), Fourier transform infrared spectrophotometer (FTIR, Nicolet-iS50), and nitrogen adsorption-desorption isotherm analyzer (Quantachrome NOVAtouch LX4). The XRD patterns were measured with CuK_α irradiation ($\lambda = 1.5406$ Å). As the reference for the measurement of DR UV-vis spectra, barium sulphate ($BaSO_4$) was used. The technique used in the FTIR spectra measurement was potassium bromide (KBr) pellets technique. Before the measurement, the sample was ground in the mortar and mixed with KBr. The sample ratio was fixed to 1:100 and it was compressed under pressure below than 2 tonnes for 5 minutes to obtain a self-supporting pellet. All the characterization measurements were carried out at room temperature, except for the nitrogen adsorption-desorption isotherm profiles, which were recorded at -196.15 °C (77 K). Prior to the measurement of the isotherm profiles, the samples were dried at 100 °C. For degassing part, the samples were heated at 180 °C for 3 hours at the ramp of 10 °C/min. The specific surface area (SA) was determined by the Brunauer-Emmett-Teller (BET) approach from the adsorption part, while the pore diameter (PD) and pore volume (PV) were derived by the equation from Barret-Joyner-Halenda (BJH).

Phenol (C6H6O, Scharlau Chemie, 99.5%) was used as the model of organic pollutant. The photocatalytic degradation reaction was performed in the similar way to the previous work [9]. Photocatalyst (50 mg) was first dispersed in 50 ml of 50 ppm phenol. Prior to the photocatalytic reaction, the solution was stirred continuously in the dark condition for 30 mins in order to reach the equilibrium of adsorption-desorption. The photocatalytic reaction was carried out under solar light irradiation (150 W, $\lambda > 230$ nm, I = 110, 000 Lux) for 6 hours. After completion, the solution was filtered to separate the sample. The final remaining concentration of the solution was determined by using a high-performance liquid chromatography (HPLC, Shimadzu LC-20AT) equipped with a UV detector. The final concentration of phenol was determined and the percentage of phenol degradation was calculated from the ratio of degraded phenol to its initial concentration.

RESULTS AND DISCUSSION

Effect of Precursor Amount

The effect of the precursor amount in the preparation of crystalline CN was studied, where the amount of precursor was varied at 2, 3 and 4 g. In the preliminary study, 1 g of the precursor was also investigated. However, the final product was believed to be fully decomposed as the amount of precursor was too low. The structural properties of the synthesized CN samples were characterized by XRD. Shown in Figure 1 are the XRD patterns of 2–CN, 3–CN, and

4–CN. From the diffractograms, only the 2–CN and 3–CN samples showed the presence of crystalline phase with 3–CN showed a decreased intensity. For the 2–CN sample, the crystalline peaks were observed at diffraction peaks at 2θ of 20.7 (110), 24.5 (200), 29.3 (102) and 32.4° (210). Meanwhile, the interlayer distance of graphite-like of CN and in-plane arrangement of nitrogen-linked heptazine CN heterocycle can be observed at 2θ of *ca.* 26.5 (002) and 11.8° (100), which gave *d*-spacing values of 0.33 and 0.74 nm, respectively. For the 3–CN sample, the crystalline peaks were observed at 2θ of 21.1 (110), 24.6 (200), 29.4 (102) and 32.1° (210). The broad and intense peaks at 27.1 (002) and 12.3° (100) were corresponded to an interlayer distance of CN and to the in-plane arrangement of CN heterocycle, which gave *d*-spacing values of 0.33 and 0.72 nm. For the 4–CN, no crystalline peak was observed but the diffraction peaks at 2θ of 27.2 and 11.9° could be detected. These peaks corresponded to the interlayer distance of graphite-like of CN and in-plane arrangement of nitrogen-linked triazine CN heterocycle, which gave *d*-spacing values of 0.33 and 0.74 nm, respectively. The XRD patterns of samples with crystalline [10-13] and amorphous phase [14-18] were in good agreement to the previous studies when the CN was synthesized by urea or other organic nitrogen-rich compounds such as melamine, dicyandiamide and cyanamide.

As presented in Fig. 1(b), increasing the amount of precursor to 3 g caused the decrease in crystallinity as well as induced back to the amorphous phase when the amount of 4 g was used (Fig. 1(c)). This result suggested that 2 g was the optimum amount of precursor needed. The decrease in the crystallinity observed on the 3–CN sample would be due to the insufficient amount of salt melts (ionic solvent) when the amount of precursor was increased. The (002) peak was also slightly shifted to the larger angle, suggesting the decrease in the interlayer distance between the CN graphitic layer. The shifting to the larger angle could be related to the decrease in crystallite size owing to the decrease in crystallinity. In addition to the crystallinity, it was reported that the (002) peak for poly(triazine imide) lies at *ca.* 26.5° [10,11,19], while heptazine–base unit has a diffraction peak of (002) plane at 2θ of 27.1° [11,19]. Therefore, the shifting to larger angle might also an indication for the presence of heptazine-based unit or tri-*s*-triazine rather than poly(triazine imide) or triazine [19].

Since the presence of heptazine-based unit or tri-*s*-triazine suggested the presence of amorphous phase, it can be suggested that the 3–CN sample consisted of a more amorphous phase and reduced crystalline phase than the 2–CN. On the other hand, the 4–CN sample showed only the amorphous phase. The decreased intensity on (002) plane might be due to excessive washing process during the removal of excess KCl-LiCl salt melt. The excessive washing process involved repeated and multiple steps of washing of the sample with distilled and boiling water with continuous stirring up to 2 hours. This procedure could affect the structural order of CN. This result suggested the need for optimum amount of precursor in order to maintain the crystallinity of the CN.

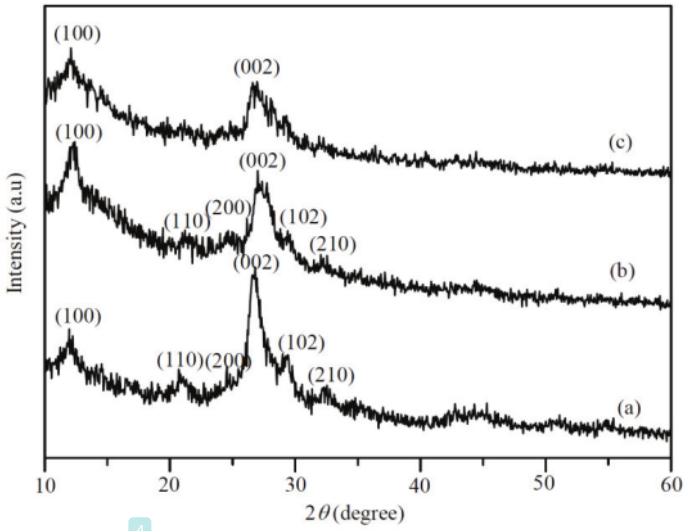

FIGURE 1. XRD patterns of (a) 2–CN (b) 3–CN and (c) 4–CN samples

The absorption properties of all the prepared CN photocatalysts were analysed by DR UV-Vis spectrophotometer. Figure 2(a) revealed the absorption spectra of 2–CN, 3–CN, and 4–CN. From the DR UV-Vis spectra, it was demonstrated that the higher the crystallinity, the higher the light absorption. For the 2–CN and the 3–CN samples, there were three main peaks were observed at the wavelength of 275, 320 and 373 nm. On the other hand, two major peaks were observed for the 4–CN sample, which appeared at the wavelength of 291 and 335 nm. The absorption peaks at 275 and 373 nm were likely to be attributed to the transition of $\pi \rightarrow \pi^*$ and $n \rightarrow \pi^*$ due to the bonds of C=N and C–N, respectively, owing to the electronic transition of aromatic heptazine/poly(triazine imide) units. The peak at *ca.* 320 nm corresponded to the transition of $n \rightarrow \pi^*$ due to the existence of C=O bond [20-22]. The formation of C=O in CN was likely due to the incomplete condensation of precursor during the polymerization process [15]. It was demonstrated that the peak intensity at 320 nm corresponded to C=O functional group on the 3–CN sample was increased, suggesting the increase in the incomplete condensation process.

All the samples showed a different edge of absorption to each other. The 2–CN sample showed the absorption up to 460 nm, followed by the 3–CN with absorption up to 450 nm. The 4–CN showed the lowest absorption range with up to 400 nm, but demonstrated a slight increase of absorption intensity at *ca.* 420–600 nm. The small upshift absorption could be caused by the formation of defects resulting from the excessive washing of the samples during the removal of excess salt melts. The excessive washing might result in a disturbance of the CN network, leading to the formation of more defects in the structure. It was reported that such defects would scatter light that resulted in a better reflection of light [14, 23].

The optical band gap energy values of the prepared samples were estimated via Tauc plot by plotting the $(\alpha h\nu)^{1/2}$ versus hν and the plot was presented Fig. 2(b). The Eg values of the respective samples are shown as the values in the *x* axis obtained from the linear extrapolation. The Eg values were altered when increasing the amount of the precursor. The Eg values were estimated to be 2.82, 2.96 and 3.19 eV for 2–CN, 3–CN and 4–CN, respectively. The increased band gap energy on the 4–CN sample was resulted from the formation of more defects and destroyed structure. These values suggested the need of optimum amount of precursor to prepare the crystalline CN in order to maintain the band gap energy value to enable them acting as visible light-driven photocatalysts.

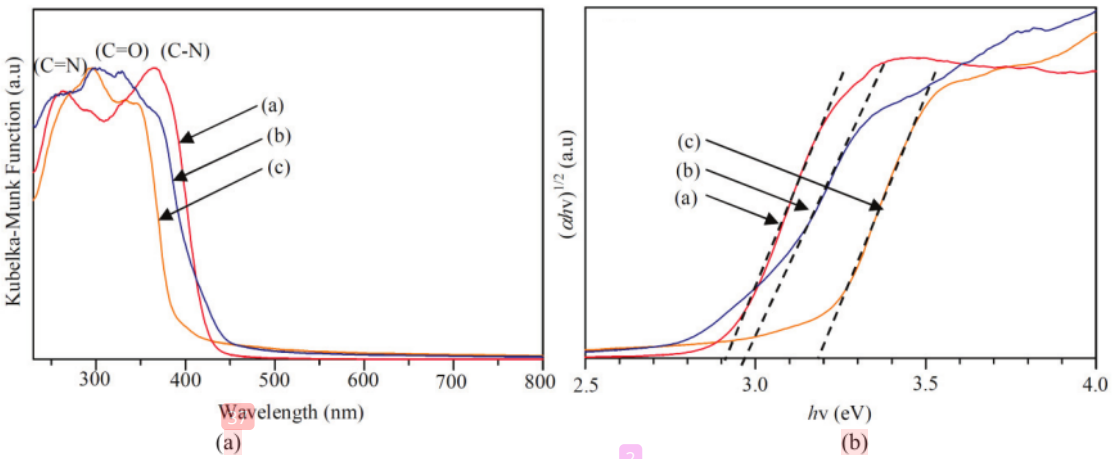

FIGURE 2. (a) DR UV-Vis spectra and (b) Tauc plots of (a) 2–CN (b) 3–CN and (c) 4–CN samples

The characteristic of the chemical bonding and functional groups of the prepared samples were investigated by FTIR spectrophotometer. Figure 3 shows the FTIR spectra of 2–CN, 3–CN and 4–CN samples. From the spectra, the formation of CN heterocycles or triazine units could be observed from the vibration band of all samples at the region of *ca.* 800 and 1200–1700 cm^{-1}. The region at *ca.* 800 cm^{-1} was assigned to bending mode of out-of-plane triazine units, while the multiple bands at *ca.* 1200–1700 cm^{-1} were corresponded to stretching mode of triazine units and tri-*s*-triazine units [10-12,14,15]. On the other hand, the small intense peak presented at *ca.* 2170 cm^{-1} observed in all samples indicated the formation of C≡N and N=C=N. The formation of both C≡N and N=C=N were typical for CN with crystalline materials due to intercalation of lithium and chloride ions in CN networks during the crystallization

process. It also implied that the continuity of CN network was disturbed [10-12]. Although the 4–CN sample was amorphous, it also showed the presence of both C≡N and N=C=N, suggesting that the continuous structure or polymer of CN was broken. The broken structure might be related to the excessive washing during removal of excess salt melts in the sample. The functional group O–H at region *ca.* 3000–3800 cm^{-1} indicated the adsorbed water molecules in all the CN samples.

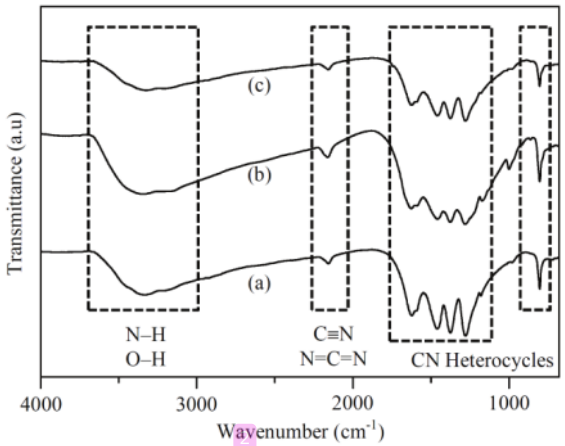

FIGURE 3. FTIR spectra of (a) 2–CN (b) 3-CN and (c) 4-CN samples

Figure 4 shows the isotherm profiles and BJH pore size distribution (shown in the inset) of the 2–CN, 3–CN and 4–CN. Based on the isotherms, the 2–CN and the 3–CN have type IV isotherm with H3 hysteresis according to IUPAC classification, suggesting the presence of the porous structure. However, the 4–CN showed a type III isotherm with no hysteresis loop. The BET specific surface area values for 2–CN, 3–CN and 4–CN were 73, 55 and 15 m^2 g^{-1}, respectively. The pore size distribution for each sample based on the increasing amount of precursors was 3.62, 3.63 and *ca.* 12 nm, respectively. It is noted that the 4–CN sample showed a broad pore distribution, where the presence of pores might be due to the formation of cavities resulting from the releases of gases (NH_3) during the polymerization process as also reported elsewhere [17]. The decrease in the BET specific surface area values might be due to the decrease in crystallinity [11]. It would be also due to the possibility of the broken structure of CN networks as can be seen on the 4–CN, which showed a big drop in the BET specific surface area to 15 m^2 g^{-1}. The reason for the similar pore size distribution values for both 2–CN and 3–CN were due to the fixed amount of salt melts added to the samples as the formation of porous was resulted from the presence of void channels due to the ABA stacking of crystalline CN [13].

The photocatalytic performance of the prepared CN samples was tested for the degradation of phenol under solar light irradiation for 6 hours. The percentages of the photocatalytic degradation along with the physical and chemical properties of the samples are listed in Table 1. As presented in Table 1, the 2–CN showed the highest activity compared to others with 24% of phenol degradation after 6 hours under solar light irradiation, while the 3–CN and the 4–CN only showed 12 and 5% degradation, respectively. Based on the physical and chemical properties presented in Table 1, it was obvious that the high photocatalytic activity achieved on the 2–CN was due to its high crystallinity and large BET specific surface area as crystallinity could provide an efficient electron charge transfer and high surface area could give many active sites for photocatalytic oxidation to occur. For the 3–CN, the decreased photocatalytic activity to almost half of that on the 2–CN was due to decreased crystallinity and BET specific surface area. However, the band gap energy did not much affect the photocatalytic activity as its value was almost close to that of the 2–CN. On the other hand, the low photocatalytic activity obtained on the 4–CN was clearly due to its amorphous phase, large band gap energy and low surface area. These results suggested the importance of crystallinity, high surface area and low band gap energy to prevent the degradation percentage from dropping to a low value.

TABLE 1. Properties and percentage of phenol degradation after 6 hours under solar light irradiation for g–CN samples

Sample	Crystallinity	E_g[a] (eV)	S.A[b] ($m^2 g^{-1}$)	Degradation (%)
2–CN	✓	2.82	73	24
3–CN	✓	2.96	55	12
4–CN	×	3.19	15	5

[a]Band gap energy values were determined via Tauc plot.
[b]Specific surface areas were determined via BET technique.

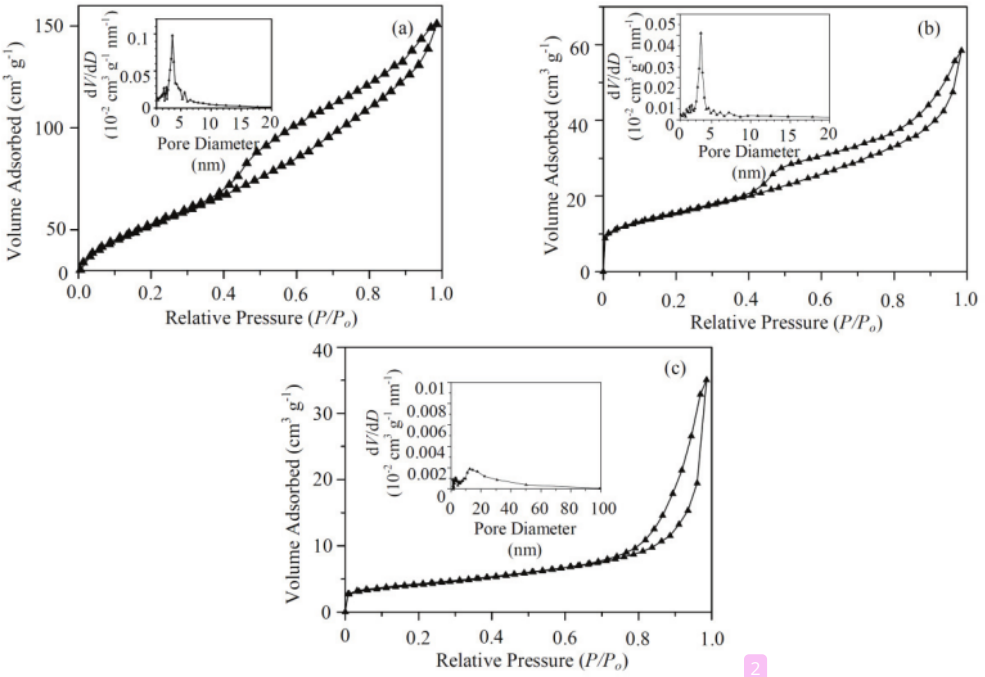

FIGURE 4. Isotherm profiles and their respective BJH pore size distribution curves (inset) of (a) 2–CN and (b) 3–CN and (c) 4–CN samples.

Effect of Salt Melts Amount

The structural properties of the synthesized CN–x photocatalysts were characterized by XRD. Based on the XRD patterns in Fig. 5, all samples showed the (002) and (100) planes that corresponded to the interlayer distance of graphite-like CN and in-plane arrangement of poly(triazine imide) and heptazine-based CN unit. Both planes could be observed at the diffraction angle of *ca.* 26.8 and 11.9°. No other peak was observed on the CN–2.5 sample (Fig. 5a). In contrast, it was observed that the CN–5 and the CN–7.5 samples showed the presence of crystalline properties. As revealed in Fig. 5(b) and 5(c), the (110), (200), (102) and (210) planes at *ca*. 20.4. 24.6, 29.3 and 32.1° were corresponded to crystalline peaks [10-18]. The CN–7.5 sample also showed the presence of unfavoured impurities (Fig. 5(c)). The impurities are coming from the excess salt melt that was difficult to be removed when the amount was too high. As outlined in the experimental part, all the samples were washed with boiling water with the stirring process of 1–2 hours. The CN–7.5 sample was subjected to second wash with a similar approach but the process reduced the crystallinity. From these XRD patterns, it can be proposed that 5 g was the optimum amount of salt melt required to synthesize crystalline CN with the best crystalline phase.

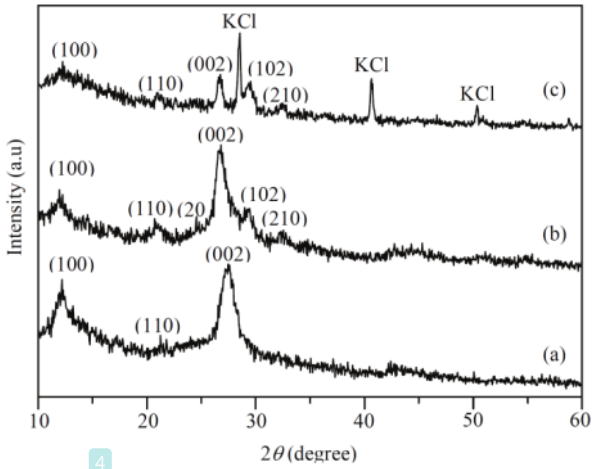

FIGURE 5. XRD patterns of (a) CN–2.5 (b) CN–5 and (c) CN–7.5 samples

The absorption properties of all the prepared CN photocatalysts were analysed by DR UV-Vis spectrophotometer. The absorption spectra of the CN–2.5, the CN–5, and the CN–7.5 are shown in Fig. 6(a). All samples showed three main peaks that corresponded to C=N, C=O and C–N owing to transition of π→π+, n→π and π→π* and π→π*, respectively [11,20,24,25]. The presence of C=O was related to the formation of defect owing to the less condense product when using the urea-based precursor. Based on the absorption pattern, it can be also noted that increasing the amount of salt melt from 2.5 to 5 g led to the increase in absorption towards longer wavelength. However, a further increase to 7.5 g did not give a further increment of absorption edge wavelength. The band gap energy values of prepared samples were estimated via Tauc plot as presented in Fig. 6(b). The obtained band gap energy values for CN–2.5, CN–5 and CN–7.5 were 2.98, 2.87 and 3.0 eV, respectively. The CN–7.5 sample showed an increase in its band gap energy value, which may be caused by the slight decrease in the layer thickness due to insertion of more Li^+ and Cl^- in the layer and the presence of excess salt melt [26].

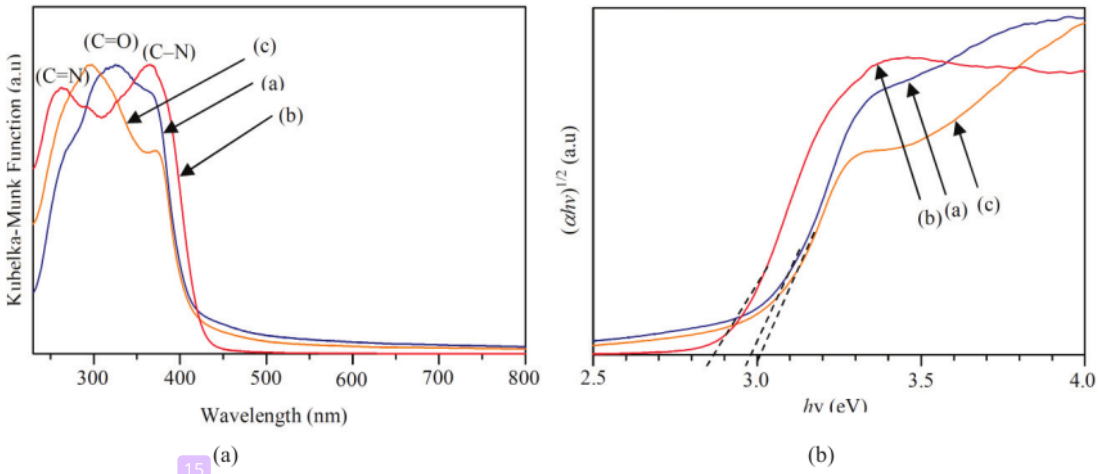

FIGURE 6. [A] DR UV-Vis spectra and [B] Tauc plots of (a) CN–2.5 (b) CN–5 and (c) CN–7.5 samples.

The characteristic of the functional groups of the samples was investigated by FTIR spectrometer. Figure 7 shows the FTIR spectra of the CN–2.5, the CN–5, and the CN–7.5. From the spectra, it can be observed that there was no significant change in the functional groups when the amount of salt melt was varied. The successful formation of CN

network can be observed from the peaks at the region of 810 and 1200–1700 cm^{-1}, which attributed to CN heterocycles. The band at 810 cm^{-1} could be assigned to the bending mode of out-of-plane heptazine-based and/or poly(triazine imide) units. Meanwhile, the bands at *ca.* 1200–1700 cm^{-1} were corresponded to the stretching mode of heptazine and/or poly(triazine imide) units. In addition, the overlapping bands of N–H and O–H groups could be observed as the broad and wide bands at region of *ca.* 3000–3700 cm^{-1} [10-2,14-17,26]. The small and intense single peak appeared at region *ca.* 2170 cm^{-1} was due to the broke of CN continuity framework [10-12, 14, 15], owing to the intercalation by both Li^+ and Cl^- ions in the crystalline CN. However, it can be noted that the peak attributed to C≡N and N=C=N at 2170 cm^{-1} for CN–2.5 sample (Fig. 7(a)) was less intense compared to others (Fig. 7(b) and (c)) due to the less amount of salt melts added.

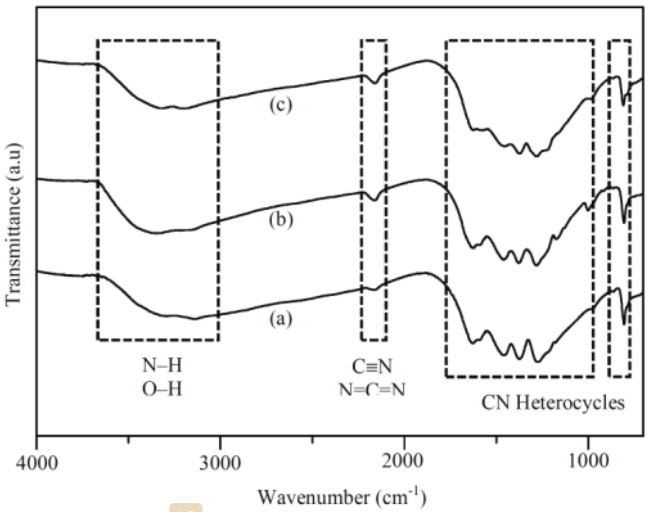

FIGURE 7. FTIR spectra of (a) CN–2.5, (b) CN–5, and (c) CN–7.5 samples.

Figure 8 reveals the isotherm profiles of nitrogen adsorption-desorption and BJH pore size distribution (inset) of the CN–2.5, the CN–5, and the CN–7.5. All samples showed the type IV isotherm with type H3 hysteresis loop, suggesting the formation of the porous structure. The values of the BET specific surface area for the CN–2.5, the CN–5, and the CN–7.5 were 60, 73, and 11 $m^2 g^{-1}$, respectively. From the insets of Fig. 8, the BJH pore size distribution analysis showed that the CN–2.5, the CN–5, and the CN–7.5 samples have an average pore size of 3.64, 3.62 and 3.63 nm, respectively. Meanwhile, the average pore volume for the CN–2.5, the CN–5, and the CN–7.5 were 0.03, 0.23 and 0.11 cc g^{-1}.

From the obtained BET specific surface area values, it could be demonstrated that the specific surface area of samples increased as increasing the salt melt amount from 2.5 to 5 g. The large surface area can be related to the high crystallinity phase of the prepared samples. However, increasing addition of eutectic mixture to 7.5 g caused a decrease in the specific surface area down to 11 from 73 $m^2 g^{-1}$. The decrease in the specific surface area of the CN–7.5 sample was due to the decrease in the crystallinity and the presence of salt melts that affected the measurement of the surface area. In addition, the decreased surface area could be associated to the destroyed CN framework due to the excessive washing of the sample. From this study, it was demonstrated that that the large specific surface area could be obtained by increasing the crystallinity. The larger amount of salt melt caused further washing process which could result in the lower crystallinity and lower specific surface area.

Table 2 shows the percentage of phenol degradation of the prepared CN–g samples after 6 hours of irradiation. From the Table, the CN–2.5, the CN–5, and the CN–7.5 showed percentage degradation of 14, 24 and 11%, respectively. It could be clearly observed that the high photocatalytic activity on the CN–5 was due to its high crystallinity, improved specific surface area and low band gap energy. The lower activities obtained on the CN–2.5 and CN–7.5 would be caused by the lower crystallinity, the presence of impurities, lower specific surface area, and higher band gap energy. These results again demonstrated that the high crystallinity, large specific surface area and low band gap energy are the key properties that lead to good photocatalytic activity.

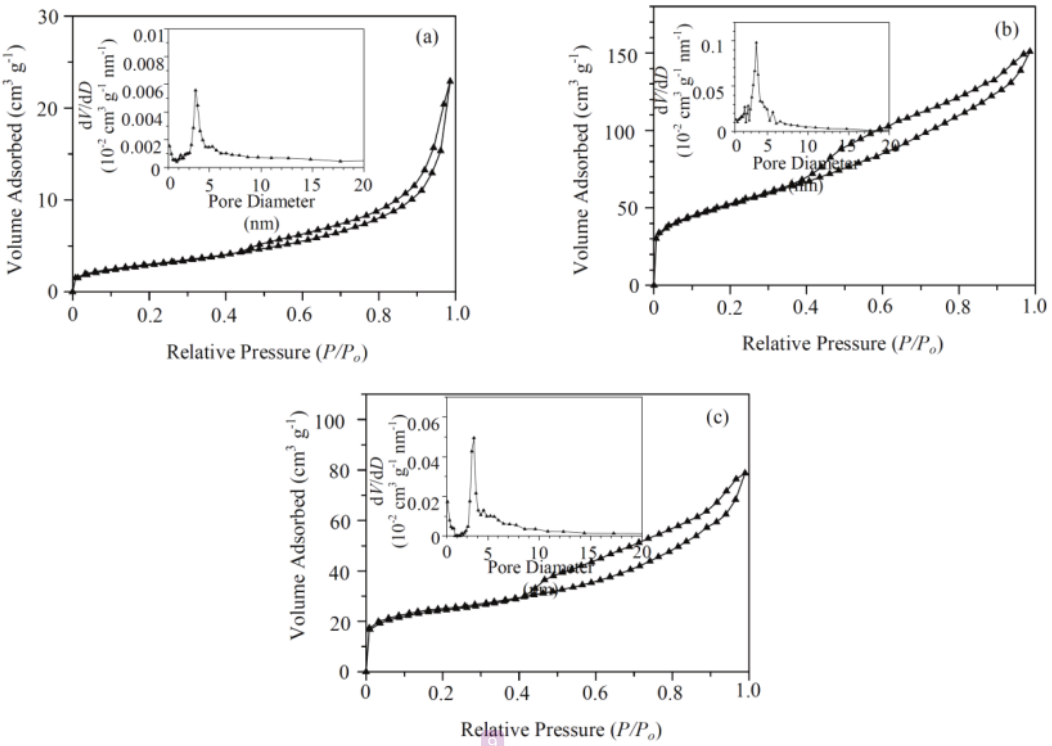

FIGURE 8. Isotherm profiles and their respective BJH pore size distribution curves (inset) of (a) CN–2.5, (b) CN–5, and (c) CN–7.5 samples.

TABLE 2. Properties and percentage of phenol degradation after 6 hours under solar simulator irradiation for CN–*g* samples

Sample	Crystallinity	Eg[a] (eV)	S.A[b] (m^2 g^{-1})	Degradation (%)
CN–2.5	×	2.98	60	14
CN–5	✓	2.82	73	24
CN–7.5	✓	3.0	11	11

[a]Band gap energy values were determined via Tauc plot.
[b]Specific surface areas were determined via BET technique.

CONCLUSION

Amounts of precursor and salt melt affected the physicochemical properties and photocatalytic performance of the crystalline carbon nitride. When the amount of the precursor was varied into 2, 3 and 4 g, it was obtained that 2 g gave the best photocatalyst properties, namely highest crystallinity, lowest band gap energy, and largest specific surface area. These properties made the 2–CN sample have the best photocatalytic activity (24%). When the amount of the salt melt was varied into 2.5, 5 and 7.5 g, the best photocatalyst properties and photocatalytic activity could be found in the CN–5 sample. Similar to the 2–CN sample, the CN–5 sample gave good crystallinity, suitable low band gap energy, and high specific surface area. This study demonstrated that the amounts of precursor and salt melt are important parameters in synthesizing the crystalline carbon nitride.

ACKNOWLEDGMENTS

Support from Directorate General of Strengthening Research and Development, Ministry of Research, Technology and Higher Education of the Republic of Indonesia via the Fundamental Research scheme (PD 2019, No. 058/SP2H/LT/MONO/L7/2019 and No. 001/MACHUNG/LPPM/SP2H-LIT-MONO/III/2019) is greatly acknowledged.

REFERENCES

1. U.S. Department of Health and Human Services, Public Health Service, Agency for Toxic Substances and Disease Registry, Toxicological Pofile for Phenol (2008).
2. G. Busca, S. Berardinelli, C. Resini and L. Arrighi, J. Hazard. Mater **160**, 265–288 (2008).
3. S. Ahmed, M. G. Rasul, W. N. Martens, R. Brown and M. A. Hashib, Desalination **261**, 3–18 (2010).
4. P. Chowdhury, S. Nag and A. K. Ray, "Degradation of Phenolic Compounds Through UV and Visible-Light-Driven Photocatalysis: Technical and Economic Aspects" in *Phenolic Compounds-Natural Sources, Importances, and Aplications*, edited by M. Soto-Hernandez, M. Palma-Tenango and M.R. Garcia-Mateos (Intech Open, 2017), pp. 395–417.
5. X. Wang, S. Blechert and M. Antonietti, ACS Catal **2**, 1596–1606 (2012).
6. Y. Wang, X. Wang and M. Antonietti, Angew. Chem. Int. Ed **51**, 68–89 (2012).
7. Y. Gong, M. Li, H. Li and Y. Wang, Green Chem. **17**, 715–736 (2015).
8. K. Schwinghammer, M. B. Mesh, V. Duppel, C. Ziegler, J. Senker and B. V. Lotsch, J. Am. Chem. Soc **136,** 1730–133 (2014).
9. M. H. M. Hatta, H. O. Lintang, S. L. Lee and L. Yuliati, Turk. J. Chem. **43**, 63–72 (2019).
10. M. J. Bojdys, J. O. Müller, M. Antonietti and A. Thomas, Chem. European J. **14** (27), 8177–8182 (2008).
11. M. K. Bhunia, K. Yamauchi and K. Takanabe, Angew. Chem. Int. Ed. **53** (41), 11001–11005 (2014).
12. K. Schwinghammer, B. Tuffy, M. B. Mesch, E. Wirnhier, C. Martineau, F. Taulelle and B. V. Lotsch, Angew. Chem. Int. Ed. **52** (9), 2435–2439 (2013).
13. E. Wirnhier, M. Döblinger, D. Gunzelmann, J. Senker, B. V. Lotsch and W. Schnick, Chem. European **17**(11), 3213–3221 (2011).
14. S. C. Lee, H. O. Lintang and L. Yuliati, Chem. An Asian J. **7** (9), 2139–2144 (2012).
15. J. Liu, T. Zhang, Z. Wang, G. Dawson and W. Chen, J. Mater. Chem. **21** (38), 14398–14401 (2011).
16. Y. Zhang, J. Liu, G. Wu and W. Chen, Nanoscale **4** (17), 5300–5303 (2012).
17. Y. Zhang, N. Zhang, Z. R. Tang and Y. J. Xu, ACS Nano **6** (11), 9777–9789 (2012).
18. J. Zhu, P. Xiao, H. Li and S. A. Carabineiro, ACS Appl. Mater. Interf. **6** (19), 16449–16465 (2014).
19. A. Jin, Y. Jia, C. Chen, X. Liu, J. Jiang, X. Chen and F. Zhang, J. Phys. Chem. C. **121** (39), 21497–21509 (2017).
20. N. S. Alim, H. O. Lintang and L. Yuliati, J. Teknol. **76** (13), 1–6 (2015).
21. F. Hussin, H. O. Lintang and L. Yuliati, Malay. J. Anal. Sci. **20** (1), 102–110 (2016).
22. S. M. Jasman, H. O. Lintang, S. L. Lee and L. Yuliati, Malay. J. Fund. Appl. Sci. **14** (1-2), 174–178 (2018).
23. Y. Cui, F. Huang, X. Fu and X. Wang, Catal. Sci. Technol. **2** (7), 1396–1402 (2012).
24. M. S. Sam, H. O. Lintang, M. M. Sanagi, S. L. Lee and L. Yuliati, Spectrochim. Acta A. **124,** 357–364 (2014).
25. P. Tiong, H. O. Lintang, S. Endud and L. Yuliati, RSC Adv. **5**, 94029–94039 (2015).
26. M. Shalom, S. Inal, C. Fettkenhauer, D. Neher and M. Antonietti, J. Am. Chem. Soc. **135** (19), 7118–7121 (2013).

AIP2020_2

ORIGINALITY REPORT

20%	10%	17%	2%
SIMILARITY INDEX	INTERNET SOURCES	PUBLICATIONS	STUDENT PAPERS

PRIMARY SOURCES

1	Hendrik O. Lintang, Mohamad Azani Jalani, Leny Yuliati. "Thermal hydrogen reduction for preservation of mesoporous silica film nanocomposites with a hexagonal structure containing amphiphilic triphenylene", AIP Publishing, 2017 Publication	2%
2	Dominik Göbel, Daniel Duvinage, Tim Stauch, Boris Johannes Nachtsheim. "Nitrile-Substituted 2-(Oxazolinyl)-Phenols: Minimalistic Excited-State Intramolecular Proton Transfer (ESIPT)-Based Fluorophores", Journal of Materials Chemistry C, 2020 Publication	1%
3	Repository.Unej.Ac.Id Internet Source	1%
4	Pandiselvi, Kannusamy, Huaifang Fang, Xiubo Huang, Jingyu Wang, Xiaochan Xu, and Tao Li. "Constructing a novel carbon nitride/polyaniline/ZnO ternary heterostructure with enhanced photocatalytic	1%

performance using exfoliated carbon nitride nanosheets as supports", Journal of Hazardous Materials, 2016.
Publication

5	Submitted to Asia Metropolitan University Student Paper	1 %
6	www.sciencegate.app Internet Source	1 %
7	123dok.com Internet Source	1 %
8	www.xdhg.com.cn Internet Source	1 %
9	Zhenyu Wang, Wei Guan, Yanjuan Sun, Fan Dong, Ying Zhou, Wing-Kei Ho. " Water-assisted production of honeycomb-like g-C N with ultralong carrier lifetime and outstanding photocatalytic activity ", Nanoscale, 2015 Publication	1 %
10	Siah, Wai Ruu, Hendrik O Lintang, Mustaffa Shamsuddin, and Leny Yuliati. "High photocatalytic activity of mixed anatase-rutile phases on commercial TiO2 nanoparticles", IOP Conference Series Materials Science and Engineering, 2016. Publication	<1 %
11	Wee-Jun Ong, Lling-Lling Tan, Yun Hau Ng, Siek-Ting Yong, Siang-Piao Chai. " Graphitic	<1 %

	Carbon Nitride (g-C N)-Based Photocatalysts for Artificial Photosynthesis and Environmental Remediation: Are We a Step Closer To Achieving Sustainability? ", Chemical Reviews, 2016 Publication	
12	ebin.pub Internet Source	<1 %
13	s3.amazonaws.com Internet Source	<1 %
14	www.beilstein-journals.org Internet Source	<1 %
15	hehong.rcees.ac.cn Internet Source	<1 %
16	www.scientific.net Internet Source	<1 %
17	Agnes Dyah Novitasari Lestari, Mudasir, Dwi Siswanta, Ronny Martien. "Determination of the optimum composition to produce minimum particle size of β-carotene microencapsulated in acid hydrolyzed starch-chitosan/TPP (tripolyphosphate) matrices using Taguchi method", AIP Publishing, 2020 Publication	<1 %
18	Ailing Jin, Yushuai Jia, Changfeng Chen, Xin Liu, Junzhe Jiang, Xiangshu Chen, Fei Zhang.	<1 %

"Efficient Photocatalytic Hydrogen Evolution on Band Structure Tuned Polytriazine/Heptazine Based Carbon Nitride Heterojunctions with Ordered Needle-like Morphology Achieved by an In Situ Molten Salt Method", The Journal of Physical Chemistry C, 2017
Publication

---

19 J.Y. Loke, R.S. Mohd Zaki, H.D. Setiabudi. "Photocatalytic degradation of methylene blue using ZnO supported on wood waste-derived activated carbon (ZnO/AC)", Materials Today: Proceedings, 2022 <1%
Publication

---

20 Sam, Mei Shie, Peggy Tiong, Hendrik O. Lintang, Siew Ling Lee, and Leny Yuliati. "Mesoporous carbon nitride as a metal-free catalyst for the removal of aniline", RSC Advances, 2015. <1%
Publication

---

21 Yehezkiel Steven Kurniawan, Kristine Anggraeni, Renny Indrawati, Leny Yuliati. "Selective betalain impregnation from red amaranth extract onto titanium dioxide nanoparticles", AIP Publishing, 2019 <1%
Publication

---

22 L Yuliati, S Z M So'ad, N S Alim, H O Lintang. "Fluorescence Sensing of Nitrite Ions on <1%

Polyvinylpyrrolidone/Zinc Oxide Composites Prepared by Impregnation Method", IOP Conference Series: Materials Science and Engineering, 2017
Publication

---

23 Wynona A. Nimpoeno, Hendrik O. Lintang, Leny Yuliati. "Zinc Oxide with Visible Light Photocatalytic Activity Originated from Oxygen Vacancy Defects", IOP Conference Series: Materials Science and Engineering, 2020
Publication

<1 %

---

24 Guohui Tian, Honggang Fu, Liqiang Jing, Baifu Xin, Kai Pan. " Preparation and Characterization of Stable Biphase TiO Photocatalyst with High Crystallinity, Large Surface Area, and Enhanced Photoactivity ", The Journal of Physical Chemistry C, 2008
Publication

<1 %

---

25 iloencyclopaedia.org
Internet Source

<1 %

---

26 Chang Xu, Zehua Jin, Jun Yang, Fan Guo, Pan Wang, He Meng, Guirong Bao, Zhi Li, Chen Chen, Fenrong Liu, Ruisheng Hu. "A direct Z-scheme LaFeO3/WO3 photocatalyst for enhanced degradation of phenol under visible light irradiation", Journal of Environmental Chemical Engineering, 2021

<1 %

Publication

27	Cintia da Silva Araújo, Jefferson Luiz Gomes Corrêa, Satyanarayan Dev, Leandro Levate Macedo et al. "Influence of pretreatment with ethanol and drying temperature on physicochemical and antioxidant properties of white and red pulp pitayas dried in foam mat", Drying Technology, 2020 Publication	<1 %
28	Feng, Liang-Liang, Yongcun Zou, Chunguang Li, Shuang Gao, Li-Jing Zhou, Qiushi Sun, Meihong Fan, Huijie Wang, Dejun Wang, Guo-Dong Li, and Xiaoxin Zou. "Nanoporous sulfur-doped graphitic carbon nitride microrods: A durable catalyst for visible-light-driven H2 evolution", International Journal of Hydrogen Energy, 2014. Publication	<1 %
29	Li, J.. "Novel titanium dioxide structure templated from filter paper scales", Journal of Alloys and Compounds, 20110505 Publication	<1 %
30	Shu Chin Lee, Hendrik O Lintang, Leny Yuliati. " High photocatalytic activity of Fe O /TiO nanocomposites prepared by photodeposition for degradation of 2,4-dichlorophenoxyacetic acid ", Beilstein Journal of Nanotechnology, 2017 Publication	<1 %

31	Yabo Wang, Jindui Hong, Wei Zhang, Rong Xu. "Carbon nitride nanosheets for photocatalytic hydrogen evolution: remarkably enhanced activity by dye sensitization", Catalysis Science & Technology, 2013 Publication	<1 %
32	Yunfeng Zhu, Mingyuan Zhu, Lihua Kang, Feng Yu, Bin Dai. "Phosphotungstic Acid Supported on Mesoporous Graphitic Carbon Nitride as Catalyst for Oxidative Desulfurization of Fuel", Industrial & Engineering Chemistry Research, 2015 Publication	<1 %
33	E. Chevalier, M. Viana, C. Pouget, D. Chulia. "Influence of Process Parameters on Pellets Elaborated in a Mi-Pro High-Shear Granulator", Pharmaceutical Development and Technology, 2008 Publication	<1 %
34	Guigang Zhang, Guosheng Li, Zhi-An Lan, Lihua Lin et al. "Optimizing Optical Absorption, Exciton Dissociation, and Charge Transfer of a Polymeric Carbon Nitride with Ultrahigh Solar Hydrogen Production Activity", Angewandte Chemie International Edition, 2017 Publication	<1 %

35 Lee, Shu Chin, Norhasnita Hasan, Hendrik O. Lintang, Mustaffa Shamsuddin, and Leny Yuliati. "Photocatalytic removal of 2,4-dichlorophenoxyacetic acid herbicide on copper oxide/titanium dioxide prepared by co-precipitation method", IOP Conference Series Materials Science and Engineering, 2016.
Publication
<1%

36 Mohammad Ziaur Rahman, Kenneth Davey, Shi-Zhang Qiao. "Carbon, nitrogen and phosphorus containing metal-free photocatalysts for hydrogen production: progress and challenges", Journal of Materials Chemistry A, 2018
Publication
<1%

37 Muhammad Riza Ghulam Fahmi, Yehezkiel Steven Kurniawan, Leny Yuliati, Hendrik O. Lintang. "Selective optical chemosensors of Fe3+ ions using 1H-indole-2,3-dione", AIP Publishing, 2019
Publication
<1%

38 Siddulu N. Talapaneni. "Synthesis of Nitrogen-Rich Mesoporous Carbon Nitride with Tunable Pores, Band Gaps and Nitrogen Content from a Single Aminoguanidine Precursor", ChemSusChem, 04/2012
Publication
<1%

39	ir.rcees.ac.cn Internet Source	<1%
40	Djoko Hartanto, Grace Yuhaneka, Wahyu Prasetyo Utomo, Ade Irma Rozafia, Yuly Kusumawati, Wiwik Dahani, Ani Iryani. "Unveiling the charge transfer behavior within ZSM-5 and carbon nitride composites for enhanced photocatalytic degradation of methylene blue", RSC Advances, 2022 Publication	<1%
41	Fa-tang Li, Shao-jia Liu, Ya-bin Xue, Xiao-jing Wang, Ying-juan Hao, Jun Zhao, Rui-hong Liu, Dishun Zhao. " Structure Modification Function of g-C N for Al O in the In Situ Hydrothermal Process for Enhanced Photocatalytic Activity ", Chemistry - A European Journal, 2015 Publication	<1%
42	Jinyuan Liu, Jia Yan, Haiyan Ji, Yuanguo Xu, Liying Huang, Yeping Li, Yanhua Song, Qi Zhang, Hui Xu, Huaming Li. "Controlled synthesis of ordered mesoporous g-C3N4 with a confined space effect on its photocatalytic activity", Materials Science in Semiconductor Processing, 2016 Publication	<1%
43	Lei Shi, Lin Liang, Fangxiao Wang, Jun Ma, Jianmin Sun. "Polycondensation of guanidine	<1%

hydrochloride into a graphitic carbon nitride semiconductor with a large surface area as a visible light photocatalyst", Catal. Sci. Technol., 2014
Publication

---

44 M.S. Azami, A.A. Jalil, N.S. Hassan, I. Hussain, A.A. Fauzi, M.A.A. Aziz. "Green carbonaceous material–fibrous silica-titania composite photocatalysts for enhanced degradation of toxic 2-chlorophenol", Journal of Hazardous Materials, 2021 <1%
Publication

---

45 Michael, Julietta Lady, Eko Adi Prasetyanto. "Hybrid PVA/alginate for extended delivery of antibiotic", AIP Publishing, 2020 <1%
Publication

---

46 Muhammad Tahir, Chuanbao Cao, Faheem K. Butt, Sajid Butt et al. "Large scale production of novel g-C3N4 micro strings with high surface area and versatile photodegradation ability", CrystEngComm, 2014 <1%
Publication

---

47 Pourdayhimi, Parisa, Pei Wen Koh, Mohamed Mohd Salleh, Hadi Nur, and Siew Ling Lee. "Zinc Oxide Nanoparticles-Immobilized Mesoporous Hollow Silica Spheres for Photodegradation of Sodium <1%

Dodecylbenzenesulfonate", Australian Journal of Chemistry, 2016.
Publication

48	Shaodong Sun, Shuhua Liang. " Recent advances in functional mesoporous graphitic carbon nitride (mpg-C N) polymers ", Nanoscale, 2017 Publication	<1 %
49	Zhang, Yan, Huifang Zhao, Zhijun Hu, Hua Chen, Xuejin Zhang, Qi Huang, Qizhong Wo, and Shiguo Zhang. "Protic Salts of High Nitrogen Content as Versatile Precursors for Graphitic Carbon Nitride: Anion Effect on the Structure, Properties, and Photocatalytic Activity", ChemPlusChem, 2015. Publication	<1 %
50	archive.pic.int Internet Source	<1 %
51	docobook.com Internet Source	<1 %
52	epdf.pub Internet Source	<1 %
53	porto.polito.it Internet Source	<1 %
54	research-repository.st-andrews.ac.uk Internet Source	<1 %

55	stksr.che.itb.ac.id Internet Source	<1%
56	www.intechopen.com Internet Source	<1%

Exclude quotes	Off	Exclude matches	Off
Exclude bibliography	On		

AIP2020_2

GRADEMARK REPORT

FINAL GRADE

/0

GENERAL COMMENTS

Instructor

PAGE 1

PAGE 2

PAGE 3

PAGE 4

PAGE 5

PAGE 6

PAGE 7

PAGE 8

PAGE 9

PAGE 10

PAGE 11